

Electromagnetic Functionalization of Wide-Bandgap Dielectric Oxides by Boron Interstitial Doping

Dae-Sung Park, Gregory J. Rees, Haiyuan Wang, Diana Rata, Andrew J. Morris, Igor V. Maznichenko, Sergey Ostanin, Akash Bhatnagar, Chel-Jong Choi, Ragnar D. B. Jónsson, Kai Kaufmann, Reza Kashtiban, Marc Walker, Cheng-Tien Chiang, Einar B. Thorsteinsson, Zhengdong Luo, In-Sung Park, John V. Hanna, Ingrid Mertig, Kathrin Dörr, Hafliði P. Gíslason, and Chris F. McConville*

A surge in interest of oxide-based materials is testimony for their potential utility in a wide array of device applications and offers a fascinating landscape for tuning the functional properties through a variety of physical and chemical parameters. In particular, selective electronic/defect doping has been demonstrated to be vital in tailoring novel functionalities, not existing in the bulk host oxides. Here, an extraordinary interstitial doping effect is demonstrated centered around a light element, boron (B). The host matrix is a novel composite system, made from discrete bulk $\text{LaAlO}_3:\text{LaBO}_3$ compounds. The findings show a spontaneous ordering of the interstitial B cations within the host LaAlO_3 lattices, and subsequent spin-polarized charge injection into the neighboring cations. This leads to a series of remarkable cation-dominated electrical switching and high-temperature ferromagnetism. Hence, the induced interstitial doping serves to transform a nonmagnetic insulating bulk oxide into a ferromagnetic ionic–electronic conductor. This unique interstitial B doping effect upon its control is proposed to be as a general route for extracting/modifying multifunctional properties in bulk oxides utilized in energy and spin-based applications.

In solid-state oxides, methods such as chemical doping/alloying,^[1–3] mechanical strain,^[4,5] defect engineering,^[6–9] and integration of distinct materials,^[10,11] have been conventionally used to control or modify a wide range of physical and chemical properties. These include the modification of the electronic band structure, conductivity, ferroelectricity, magnetism, ionic diffusion, crystal symmetry, and so on. In this regard, perovskite (ABO_3) oxides and their related heterosystems have recently received substantial attention. Extraordinary physical phenomena have been observed in artificially designed heterostructures that do not appear in their respective host oxides; namely, the coexistence of superconductivity and ferromagnetism within the buried interface between two wide-bandgap insulators, e.g., $\text{LaAlO}_3/\text{SrTiO}_3$,^[12,13] and

Dr. D.-S. Park, Dr. A. Bhatnagar
Zentrum für Innovationskompetenz SiLi-nano
06120 Halle, Germany
E-mail: dspark1980@gmail.com, daesung.park@physik.uni-halle.de

Dr. D.-S. Park, Dr. D. Rata, Dr. I. V. Maznichenko, Dr. S. Ostanin,
Dr. A. Bhatnagar, Dr. C.-T. Chiang, Prof. I. Mertig, Prof. K. Dörr
Institut für Physik
Martin-Luther-Universität Halle-Wittenberg
06120 Halle, Germany

Dr. G. J. Rees, Dr. R. Kashtiban, Dr. M. Walker, Z. Luo,
Dr. J. V. Hanna, Prof. C. F. McConville
Department of Physics
University of Warwick
Coventry CV4 7AL, UK

Dr. H. Wang
Fritz-Haber-Institut der Max-Planck-Gesellschaft
14195 Berlin, Germany

Dr. A. J. Morris
School of Metallurgy and Materials
University of Birmingham
B15 2TT Birmingham, UK

 The ORCID identification number(s) for the author(s) of this article can be found under <https://doi.org/10.1002/adma.201802025>.

Dr. S. Ostanin, Dr. C.-T. Chiang, Prof. I. Mertig
Max-Planck-Institut für Mikrostrukturphysik
06120 Halle, Germany

Prof. C.-J. Choi
School of Semiconductor and Chemical Engineering
Chonbuk National University
Jeonju 54596, Republic of Korea

R. D. B. Jónsson, E. B. Thorsteinsson, Prof. H. P. Gíslason
Science institute
University of Iceland
Reykjavik IS-104, Iceland

Dr. K. Kaufmann
Fraunhofer Center for Silicon Photovoltaics CSP
Halle 06120, Germany

Dr. I.-S. Park
Institute of Nano Science and Technology
Hanyang University
Seoul 04763, Republic of Korea

Prof. C. F. McConville
College of Science
Engineering & Health
RMIT University
Melbourne, VIC 3000, Australia

DOI: 10.1002/adma.201802025

spontaneous exotic ferromagnetic orderings and spin-orbit interactions in transition metal (TM) oxides and their integrated systems, e.g., doped manganites, with tunable magnetoresistance responses.^[1,14–20] In the case of strongly correlated systems, the inclusion of *d* and *f* orbitals of TMs, which have strong interactions between charge, spin, orbital, and lattice degrees of freedom, is traditionally a prerequisite for tailoring the newly evolved electromagnetic properties. In the field of spin-based electronics, materials with a highly tunable electromagnetic response are in intense demand for room-temperature applications and have been achieved via doping or electrical gating.^[21–24]

In contrast to the conventional substitutional doping approach, light element doping has been rarely employed due to issues pertaining to large differences in ionic radii between the dopant and the host oxide elements, coupled with low stability and tunability.^[25,26] As a result, light elements are often assumed to be interstitially positioned within the host material lattices, or at defect sites.^[27,28] However, recently the *sp*-orbital characteristics of light elements (with atomic numbers lower than oxygen) have stirred a lot of interest. The evolution of nontrivial ferromagnetic responses in TM-free light element systems, such as doped graphites, has been proposed to be centered around the associated *sp*-orbital light elements.^[29,30] Compared to the typical magnetic materials with the strongly localized nature of TM *d/f* orbitals, strong *sp*-electron delocalization and Curie temperatures well above room temperature were observed in these light element systems. This originally weak magnetism has been primarily explained as *Stoner ferromagnetism*.^[31,32] There is a high magnitude of spin-wave stiffness of *sp*-orbitals which fulfills the Stoner criterion; $N(E_F) \cdot I_{\text{eff}} > 1$, where $N(E_F)$ and $I_{\text{eff}} \approx 1$ eV are the density of one-electron state at the Fermi level (E_F) in the unsplit band of the paramagnetic ground state and an effective exchange integral, respectively. For impurity band-associated ferromagnetism in an itinerant electron system, the Stoner criterion can be satisfied only when the impurity bandwidth, W_i , is sufficiently narrow according to the relation $N(E_F) \approx n_i/W_i$, where n_i is the atomic fraction of impurity in a system. Despite the recent studies, the origin of the resultant local magnetic moments and subsequent long-range ordering are still under deliberation. In addition, other light elements, such as Li and He, have been employed in dielectrics, and ferroic material systems for modifying the degree of lattice strain, and local electronic states, although their definitive role is still unclear.^[33,34] The light element interstitial doping approach is practically still in its initial stages, without a comprehensive understanding of the associated atomic/ionic and electronic characteristics, and its impact on the properties of the host materials.

Here, we demonstrate an interstitial light element doping into bulk oxides to evoke novel multifunctional properties such as room-temperature electrical switching and ferromagnetism. Our findings show the evolution of such phenomena upon the inclusion of a light weight boron (B), which is interstitially doped into the oxide composite of the $\text{LaAlO}_3(1-x):\text{LaBO}_3(x)$. Both undoped bulk oxides are inherently nonmagnetic and insulating with bandgap energies of ≈ 5.6 and $\approx 5.4\text{--}5.9$ eV for bulk LaAlO_3 (LAO) and LaBO_3 (LBO), respectively.^[35,36] Henceforth, x will be used as the variable to denote the composition ratio of LBO to LAO in the composites. As a result, the utmost

ordering of interstitial B cations throughout the composite system triggers remarkable conductive and ferromagnetic characteristics. The observed unique interstitial B doping effect in the host oxide matrices contrasts with the conventional substitutional doping mechanisms utilizing a charge imbalance.

Three constituent binary oxides, La_2O_3 , Al_2O_3 , and B_2O_3 , were mixed to form the LABO composites. The ratios between LAO and LBO were determined by their stoichiometric relations (S1). The LABO composites, consisting of rhombohedral LAO (space group: *R-3c*) and orthorhombic LBO (*Pnma*) crystals, were synthesized as a function of LBO composition, x up to 10% as shown in **Figure 1a,b**. A subsequent thermally driven sintering process led to a thermodynamic equilibrium condition during the material synthesis. This gives rise to the formation of thermodynamically stable LABO composites that consist of phase-separated and independent LAO and LBO phases in ceramic pellet forms. The large difference in the crystal structure of rhombohedral LAO and orthorhombic LBO phases and the ionic radii of Al and B prevent any relevant substitutional B doping into the LAO lattice.^[11] The resultant LABO composite pellet samples used in this study are white in color and polycrystalline in nature, and no secondary phase formation was found. The conditions are biased for structural and atomic incompatibilities and the associated complete phase separation of LAO and LBO phases in the composite system is observed. This eventually leads to the positioning of B atoms as interstitials, which modify the inherent properties of the host LAO system. Such a strategy potentially provides an energetically favorable landscape for the B cation to diffuse into the neighboring LAO phases and settle within interstitial sites.

To investigate the nature of the B coordination environments in the LABO($x = 5\%$), 2D and T_1 magic angle spinning (MAS) solid-state nuclear magnetic resonance (NMR) studies were performed (**Figure 1c,d**—details in S1 and S2, Supporting Information). The NMR results for the LABO($x = 5\%$) composite show two overlapping resonances; the first corresponds to the LBO and the second originates from the B interstitials. The horizontal nature of the 2D triple quantum MAS (3QMAS) resonances suggest that both B environments are highly ordered without other observable phase distributions. The longitudinal spin-lattice relaxation (T_1) is a first-order time constant which is defined as when 63% of the net magnetization returns back to thermal equilibrium, the rate of this time constant is governed by the local electronic environment of the observed nuclei. The relaxation characteristics of the two resonances observed in the composite have a large variance; the slow (222 s) relaxing LBO environment has a strong correspondence with the T_1 measured for the undoped bulk LBO (238 s) and the increased relaxation rate (1.2s) of the B interstitial (B_i) environment is distinctive of a nucleus neighboring conduction electrons.^[37] Typically, a rapid spin-lattice (T_1) relaxation, at nuclei neighboring conduction electrons, is produced by the fluctuating local magnetic fields caused by the conduction electrons hyperfine coupling to the nuclear site. Consequently, our solid state NMR results conclude that the B_i environment is locally ordered throughout the system and experiences the presence of conduction electrons, whilst the LBO phase in the system remains relatively isolated from these conduction electrons. Further investigation with atomic resolution

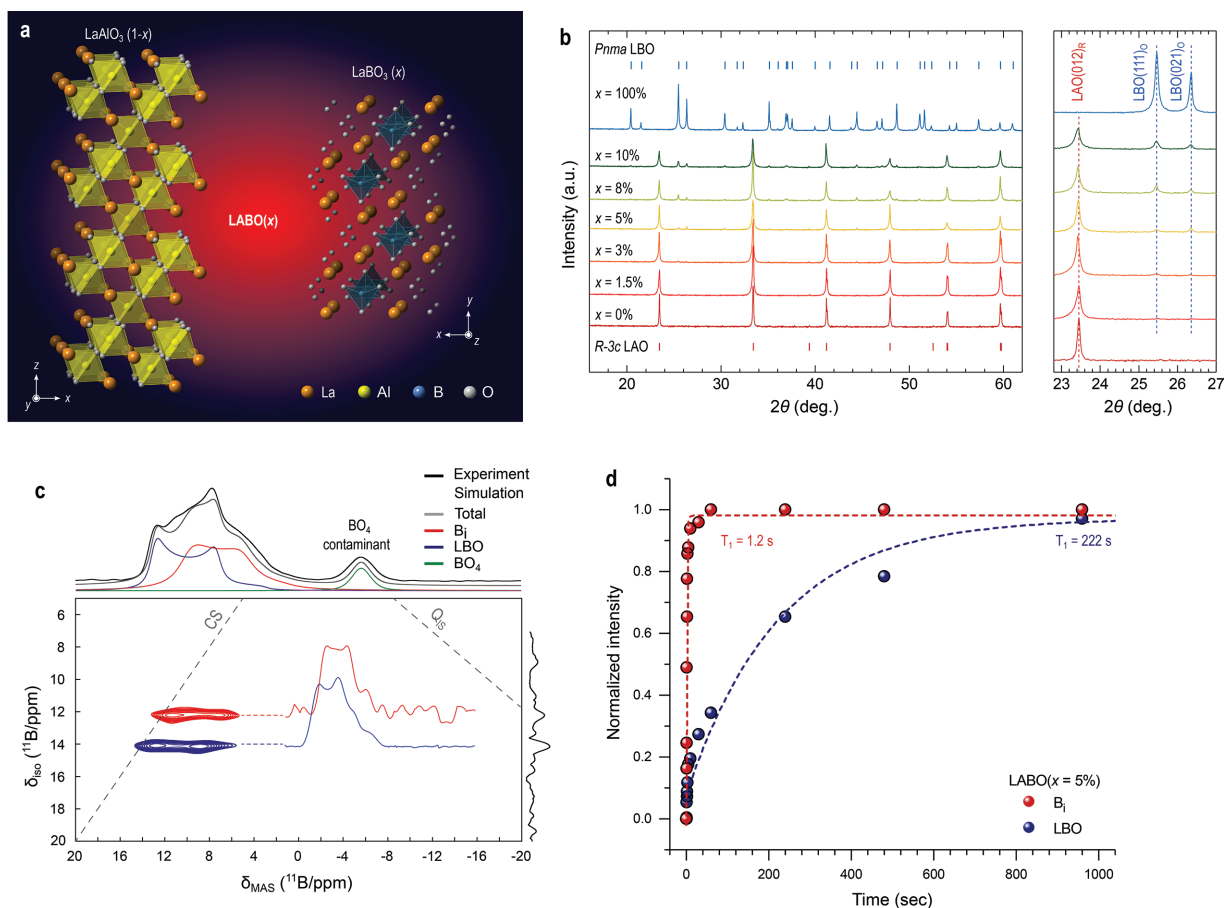


Figure 1. a) A mixture of rhombohedral $\text{LaAlO}_3(1-x)$ and orthorhombic $\text{LaBO}_3(x)$ to form $\text{LABO}(x)$ composites. The “ x ” denotes the percent quantity of LBO mixed with “ $1-x$ ” quantity of LAO to form the $\text{LABO}(x)$ ceramic pellets. b) X-ray diffraction patterns of the undoped rhombohedral ($R-3c$) LAO, orthorhombic ($Pnma$) LBO, and $\text{LABO}(x)$ composites with different LBO compositions, x (up to $x = 10\%$). c) The ^{11}B 3QMAS (12 kHz) NMR spectrum of $\text{LABO}(x = 5\%)$ displays two distinct resonances, which are extracted as 1D projections and represent the bulk LBO (blue) and B_1 (red) environments in the system. The projections of these two resonances are employed as the root of simulations of the overlaid 1D ^{11}B MAS spectrum. A recycle delay of 5 s was used to give a bias towards the minor B_1 environment. d) The saturation recovery ^{11}B NMR data for $\text{LABO}(x = 5\%)$ showing the T_1 relaxation times of LBO (blue) and B_1 (red) environments.

scanning transmission electron microscopy and X-ray photoemission spectroscopy (Figures S3 and S4, Supporting Information) correspondingly indicate distribution and positioning of the B interstitials within the LAO lattices of the composites. The subtle-strained LAO lattices in the composites are formed by ordered B_1 distributions, which is also verified by the electron energy loss spectroscopy spectrum and corroborated by XRD and NMR observations.

To evaluate the electrical characteristics of the LABO composite pellet samples, two parallel platinum (Pt) electrodes were fabricated at the surface of the composite pellet samples, separated by a gap of $\approx 80\ \mu\text{m}$ (the inset of Figure 2a). An external electric field of $\approx 12.5\ \text{kV/cm}^{-1}$ was applied across the gap through unidirectional hysteretic voltage poling up to +100 V ($0\ \text{V} \rightarrow +100\ \text{V} \rightarrow 0\ \text{V}$, at a rate of $1\ \text{V s}^{-1}$) for the purpose of electroforming (EF) process. Hereafter, the electroformed composite samples will be referred to as EF- LABO . Highly insulating behaviors were observed in the undoped LAO and LBO, with no significant change in the electric current across the gap regardless of the strength of applied external electric

fields (Figure 2a). The initial electrical state of the LABO composites also showed similar insulating characteristics in the low voltage regime (20–30 V) without any EF process (Figure S5a, Supporting Information). However, during the EF process, highly conductive channels were formed in all the LABO composites at varying set-voltages, with a sudden increase of current in the electrically poled direction. A clear dependence of the set-voltages on the composition, x , can be seen; as x increases, the set voltage required to form the high conducting channels decreases from 78 V ($x = 1.5\%$) to 37 V ($x = 10\%$). This implies that the composites with higher x possess higher population of mobile ionic species that can be readily driven by an external electric force at room temperature as schematically depicted in the inset of Figure 2b. As a result, two different conduction states, namely high resistance state (HRS) and low resistance state (LRS), were created within the LABO composites by the EF process (Figure 2b). It is noteworthy that the formation of such distinct resistance states in this composite system is fundamentally different from an anion-mediated mechanism often reported in metal oxides. For instance, in ABO_3 -type perovskite

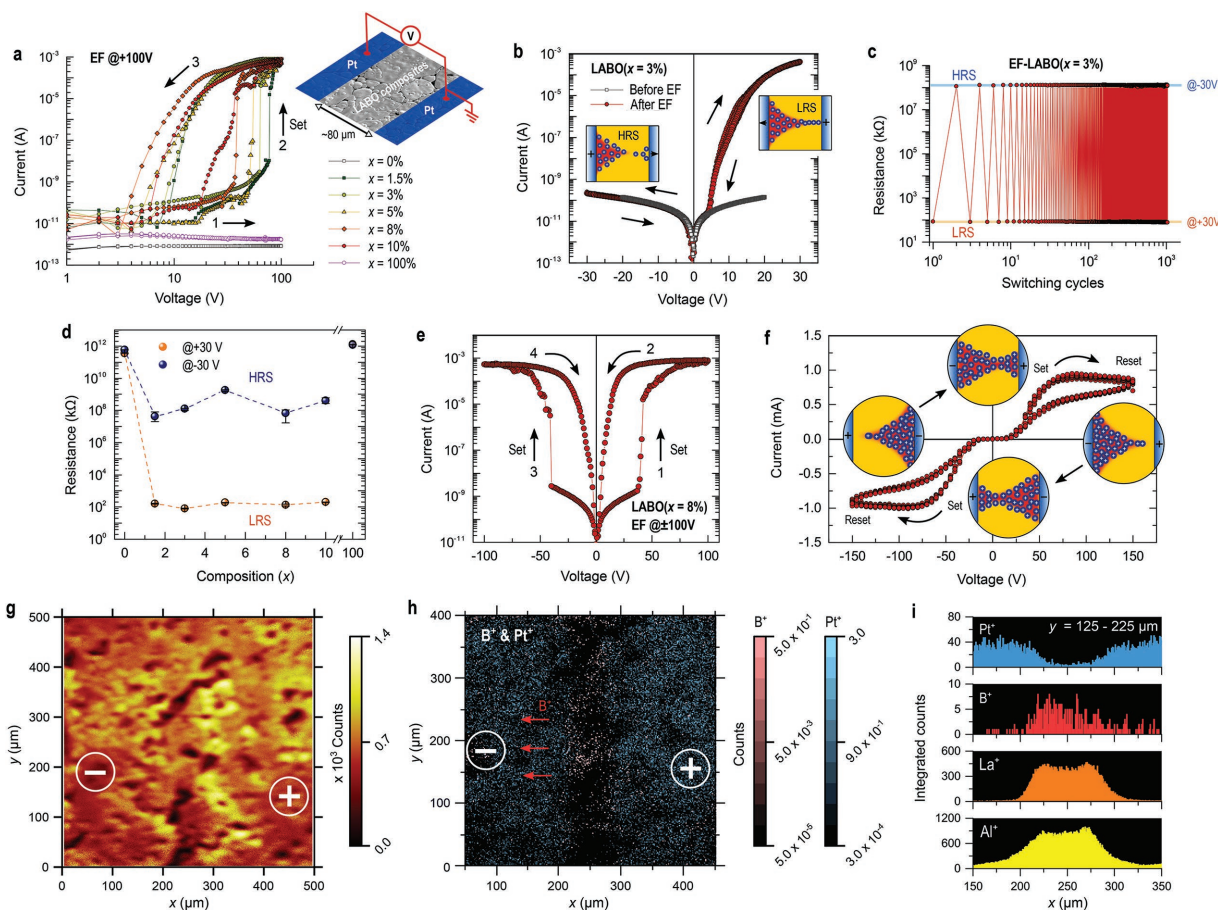


Figure 2. a) Electroforming (EF) process in the undoped LAO, LBO, and LABO(x) composites after a poling sequence, i.e., $0\text{ V} \rightarrow +100\text{ V} \rightarrow 0\text{ V}$, across a gap of $80\ \mu\text{m}$. The inset shows a schematic depicting the geometry of DC measurements with planar Pt electrodes separated by a gap of $80\ \mu\text{m}$. b) Current–voltage (I – V) curves of the LABO($x = 3\%$) composite before and after the EF process. c) The cyclic switching performance of the low (LRS) and high resistance states (HRS) of the EF-LABO($x = 3\%$) composite upon application of a $\pm 30\text{ V}$ pulse over a period of 10^3 repetition. d) LRS/HRS ratios in the undoped LAO and LBO, and EF-LABO(x) composites. e) The bipolar switching of the LABO($x = 8\%$) composite by applying hysteric high voltage sweeps of $\pm 100\text{ V}$ in a sequence (1 \rightarrow 2 \rightarrow 3 \rightarrow 4). f) 10-time I – V hysteresis curves of the composite, measured at $\pm 150\text{ V}$ at a rate of $\approx 12.5\text{ V s}^{-1}$ after the bipolar switching. The set-and-reset transition of the resistive switching is schematically depicted by a cyclic sequence of field-driven two-filament growth and gap opening during the operation. g) An electrically poled area at the surface of the LABO($x = 8\%$) composite measured by ToF-SIMS. h) 2D elementary mapping of B and Pt ions across the electrode gap. The highlighted dashed area corresponds to the dashed area within the white solid line square given in (g). The maximum scale ranges of B^+ and Pt^+ counts are adjusted for visualization of the B ion distribution across the Pt electrodes. i) The integrated counts of the detected Pt, B, La, and Al ions for the area ($x = 150\text{--}350\ \mu\text{m}$, $y = 125\text{--}225\ \mu\text{m}$).

oxides, formation of differential resistive states is usually attempted by the arrangement of anion defects (drift/diffusion of oxygen vacancies) upon overcoming high activation energies of ≈ 0.5 to $\approx 2.8\text{ eV}$, which require extremely high electric fields above few tens MV cm^{-1} or high operation temperature above $500\text{--}700\text{ K}$ or over very confined length scale (few tens or hundreds of nanometers).^[11,38]

Furthermore, with very low current flow (few tens of pA) and a near zero electric field range ($\leq 5\text{ V}$, 0.6 kV cm^{-1}) due to the $80\ \mu\text{m}$ gap distance, we observed that the LRS states, in the EF-LABO composites in the low voltage range of around 10 V , partially show Schottky-like rectifying behavior and trap-limited space charge conduction.^[39] Such additional interfacial effects on the current flow can be attributed to a large band offset with a large work function difference between the Pt electrodes and LABO composites, and pre-existing charge carrier trap centers, which typically originate from the point/planar defects

(Figures S5 and S6, Supporting Information). Nevertheless, the creation of the LRS in the composites predominantly arises from the interface modification by the rearrangement of the mobile ions across the large insulating gap after the EF process as a filamentary conduction. Accordingly, the created conducting channels overwhelmingly exhibit a nearly metallic character as verified by temperature dependent resistance measurements (Figure S5c, Supporting Information). The conducting states in the composites were persistent despite several identical EF cycles (see Figure S5e, Supporting Information), and last for more than six months without any significant degradation.

To further examine the retention properties of the conducting channels in the EF-LABO composites, intermediate reading voltages of $\pm 30\text{ V}$ were applied and consecutively switched 10^3 times, as illustrated in Figure 2c. The eventual low and high resistance states formed in the LABO($x = 3\%$) composite remain mostly consistent at $\approx 80\text{ k}\Omega$ and $1.5 \times 10^8\text{ k}\Omega$,

respectively. Such persistent states of resistance were formed in all the composites after the EF process and exhibit excellent endurance performance over the switching cycles with the HRS/LRS ratios of $\geq 10^6$ (Figure 2d and Figure S5b, Supporting Information). These results reveal the dominant role of a particular ionic component in the creation of conductive channels although quantitative evaluation of the effective doping level of the ions was difficult to determine experimentally.

The observed field-driven ionic motion and the associated changes in the resistance indeed suggest a memristive switching characteristic. To confirm this, we performed a bipolar switching of the LABO ($x = 8\%$) sample, by applying hysteric voltage sweeps of ± 100 V (Figure 2e). In the initial forming process, two set-voltages and a sudden increase in the current for both positive and negative polarities were observed. This apparently indicates a reversible ionic motion under the applied fields and the formation of an ionic memristor to switch to the LRS states. Interestingly, the subsequent switching behavior of the electro-formed composite sample shows a symmetric unipolar resistive switching (the set and reset transition) for both polarities mimicking complementary resistive switching characteristic.^[40] A mechanism for the set and reset transition can be proposed using the sequence which involves propagation of two conducting filaments across the gap (at the intermediate voltages, ± 40 – 80 V), in conjunction with the opening-up of the conducting gap (towards the formation of one conducting channel at the high fields, $> \pm 80$ V), as schematically depicted in Figure 2e. This affirms that the field-driven mobile species create two different logic states (0 and 1) corresponding to two resistance states that can be potentially stored as a nonvolatile memory for data storage applications. Such unique resistive switching features of these composites in the microscale can be practically scaled down to nanodevices, which would offer obvious advantages for operation such as low power consumption, fast switching time, high endurance, and noiseless and selectless operation.

To verify the relation between the local elementary distribution and the electrical conduction, elementary 2D mapping acquired by time-of-flight secondary ion mass spectroscopy (ToF-SIMS) is presented in Figure 2g–i. Scans were measured within the electrically poled area in the EF-LABO ($x = 8\%$) composite and the positively charged B ions migrate and accumulate with a resultant gradient in the distribution of counts from the negatively poled area. This directly indicates that the formation of the conducting channels in the composites is predominantly associated with the rearrangement of B ions.

Another interesting observation from the LABO composites is extraordinary ferromagnetic responses. Figure 3a shows field-dependent magnetization (M versus H) loops measured at 5 K under external magnetic fields, ± 50 kOe (for comparison, only the data within the range of ± 6 kOe are shown), for the composites as a function of composition, x . In all the composites, clear ferromagnetic hysteresis loops were observed, which is completely at odds with the paramagnetic response of the undoped LAO and LBO shown in the inset of Figure 3a. The diamagnetic and paramagnetic responses were cautiously subtracted from the measurements, as illustrated in Figure S7a (Supporting Information). The saturation (M_S) and remanence (M_R) magnetization of the composites steadily

increases with x , while conversely the coercivity (H_C) decreases (Figure 3b). Moreover, the magnetization remains independent of the temperature up to 400 K for all the composites. Paramagnetic upturns were measured in all the samples at temperatures below 10 K, which could be attributed with environmental paramagnetic contamination, e.g., C-based radicals or equipment accessories in the SQUID magnetometer.^[30,41] The presence of external metal impurities, e.g., Fe, Ni, and Co, was also considered. The measured M_S of all the composite samples are indeed much higher ($> \approx 1000$ times) than typical M_0 values for impurity level of a few ppm,^[42] but no elementary response and no quantitative variation for such magnetic impurities were found from any of the LABO composites with x (see Figure S8c, Supporting Information). Therefore, the increase in the magnetization of the LABO composites with x is primarily related to the enrichment of B ions and the Stoner-like ferromagnetism with a high Curie temperature.^[29] In addition, the decreased H_C of the composites with x could be associated with a size distribution effect of the B-induced ferromagnets in the composites.^[43]

To clarify the origin of the abnormal ferromagnetism, the effect of external electric stimulation on the magnetization in two different composites ($x = 3\%$ and 8%) was examined, which were initially electro-formed along the vertical direction (across top- and bottom-Pt electrodes on the samples with a gap of ≈ 500 μm for the uniform alignment of B ions – Figure 3d). The saturation magnetization of the EF-LABO composites substantially increases by ≈ 13 and 4 times for the EF-LABO ($x = 3\%$) and ($x = 8\%$), respectively, higher than that of the pristine ones (the left panel of Figure 3d). In addition, the temperature-independent magnetization reveals that the origin of the ferromagnetism in the EF-LABO composites is fundamentally identical with that of the pristine composites (the right panel of Figure 3d). Hence, the enhanced magnetization of the EF-LABO composites is due to an increment in the ferromagnetic ordering of B ions. In the M versus T curves (Figure S7b, Supporting Information), the induced and extended magnetic orderings in the EF-composites correspond to the appearance of an FC/ZFC split with their sufficient anisotropy energies at low temperatures. In contrast, no splittings were observed from the as-prepared composite samples in which superparamagnetic-like fine magnetic clusters (few nanometre sizes) are most probably randomly distributed in the polycrystalline pellet form as observed in STEM and denoted by arrows in Figure S4a,b (Supporting Information).^[44]

To emphasize the dominant role of the ordered B ions for the controlled ferromagnetism, the EF-LABO composites were thermally annealed at 600 °C for 60 min in different ambient conditions, in O_2 and in vacuum. This results in a significant lowering of the M_S by about 75%, regardless of the annealing conditions. The thermally induced magnetic degradation of the composites is primarily due to the loss of B ions ($\approx 80\%$), confirmed by SIMS depth profiling (Figure S8, Supporting Information). The SIMS results also show an almost same amount of LBO composition in the composites both before and after annealing. This reveals that excess B atoms are interstitially distributed and bound within the host matrices and can be displaced with sufficient thermal energy. Consequently, our results indicate that the ordered B interstitials are the main contributor in the evolution of the ferromagnetism of the LABO

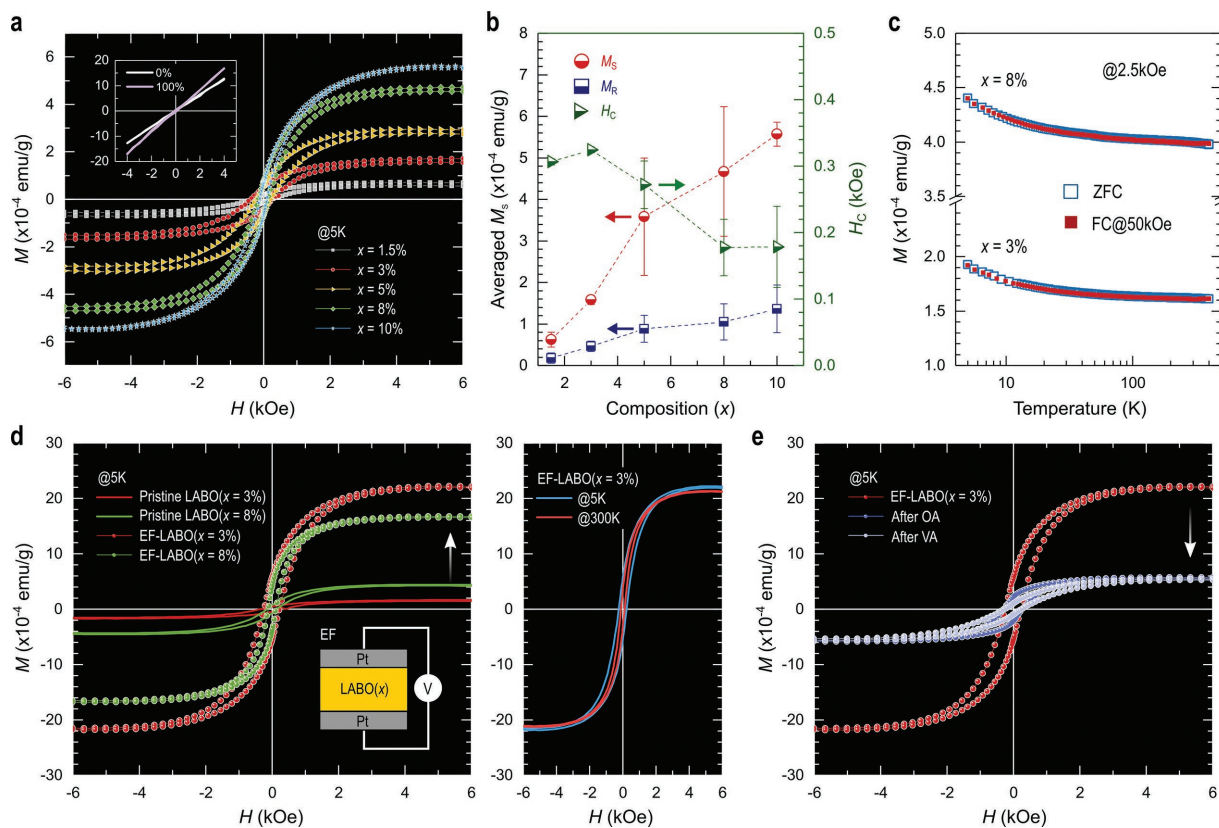


Figure 3. a) 5 K M versus H hysteresis loops of the ferromagnetic LABO(x) composites. The inset shows the M versus H hysteresis loops of the paramagnetic undoped LAO and LBO. b) Variations in the averaged saturation magnetization (M_S), magnetization remanence (M_R), and coercivity (H_C) of the composites as a function of x at 5 K. c) Temperature-dependent magnetization curves of the LABO($x = 3\%$ and 8%) composites by zero-field (ZF) and field cooling (FC) processes. In the FC process, an external magnetic field of 50 kOe was applied from RT to 5 K and the M - T curves were collected in a magnetic field of 2.5 kOe. d) 5 K M versus H hysteresis loops of the LABO($x = 3\%$ and 8%) composites before and after EF process. The right-hand panel shows the M versus H hysteresis loops of the EF-LABO($x = 3\%$) composite at different temperatures, 5 K and RT. e) The thermal annealing effect on magnetization of the EF-LABO($x = 3\%$) composite with different ambient conditions, O_2 (OA) and vacuum (VA) as measured at 5 K.

composites and play the key role in manipulating the magnetic properties of the composites. This also implicitly rules out any kind of magnetic contribution from the oxygen vacancies in the composites (see Figures S9 and S11, Supporting Information). In all the polycrystalline undoped and composite pellets, the effect of grain boundaries, native point defects (e.g. oxygen vacancies), and foreign impurities cannot be completely disregarded. However, no significant effect of such defects on variations of the properties of the undoped pellets was observed. This clearly suggests a required mutual condition; the coexistence of B interstitials and the host LAO counterparts, which creates the aforementioned extraordinary properties of the LABO composites.

To elucidate the B_i doping effect on the observed electronic and magnetic properties of LABO composites, we performed first principles density functional theory calculations. Ab initio random structure searching (AIRSS) calculations were conducted to obtain an optimal position for the B_i atom within a LAO supercell (B_i :LAO SC with $B = 0.8$ at%)^[45]—details are present in S1 and S5 in the Supporting Information. The spin-polarized and orbital-projected density of states (DOS) of the optimized B_i :LAO SC show that the highest valence band states are comprised of mainly O p -states, while the states at the

conduction band minimum are dominated by the La d - and f -states, as illustrated in Figure 4c. Three new sharp peaks mostly attributed to the partial s -states and p -states of the B_i appear in the bandgap near the Fermi level (E_F) for the B_i :LAO structure (Figure 4d). The integrated DOS indicates that the first and second peaks near $E = -1$ eV add exactly one spin-up electron and one spin-down electron into the system, respectively (Figure S10a, Supporting Information). The third spin-up electron originates totally from the B p -states and appears marginally below the E_F . More interestingly, the electronic states of B are hybridized with the nearest neighboring host atoms, La and O, which give rise to repetition of the induced spin character. This can be observed as minor peaks within the bandgap for both La and O (Figure 4f, and Figure S10a in the Supporting Information). As illustrated in Figure 4a,b, the residual delocalized single electron provided by the p -states of the B_i in the LAO SC is partially transferred into the neighboring La (0.23e) and O (0.12e) atoms, respectively. The total excessive charge induced by the B_i is 0.99e and the local charge density of the system is $\rho = 1.80 \times 10^{-2} e \text{ \AA}^{-3}$. As a result, the electrons transferred from the B to the neighboring La and O atoms are spin-polarized, leading to the magnetization of the system with the total magnetic moment of $1 \mu_B$. This is primarily driven by

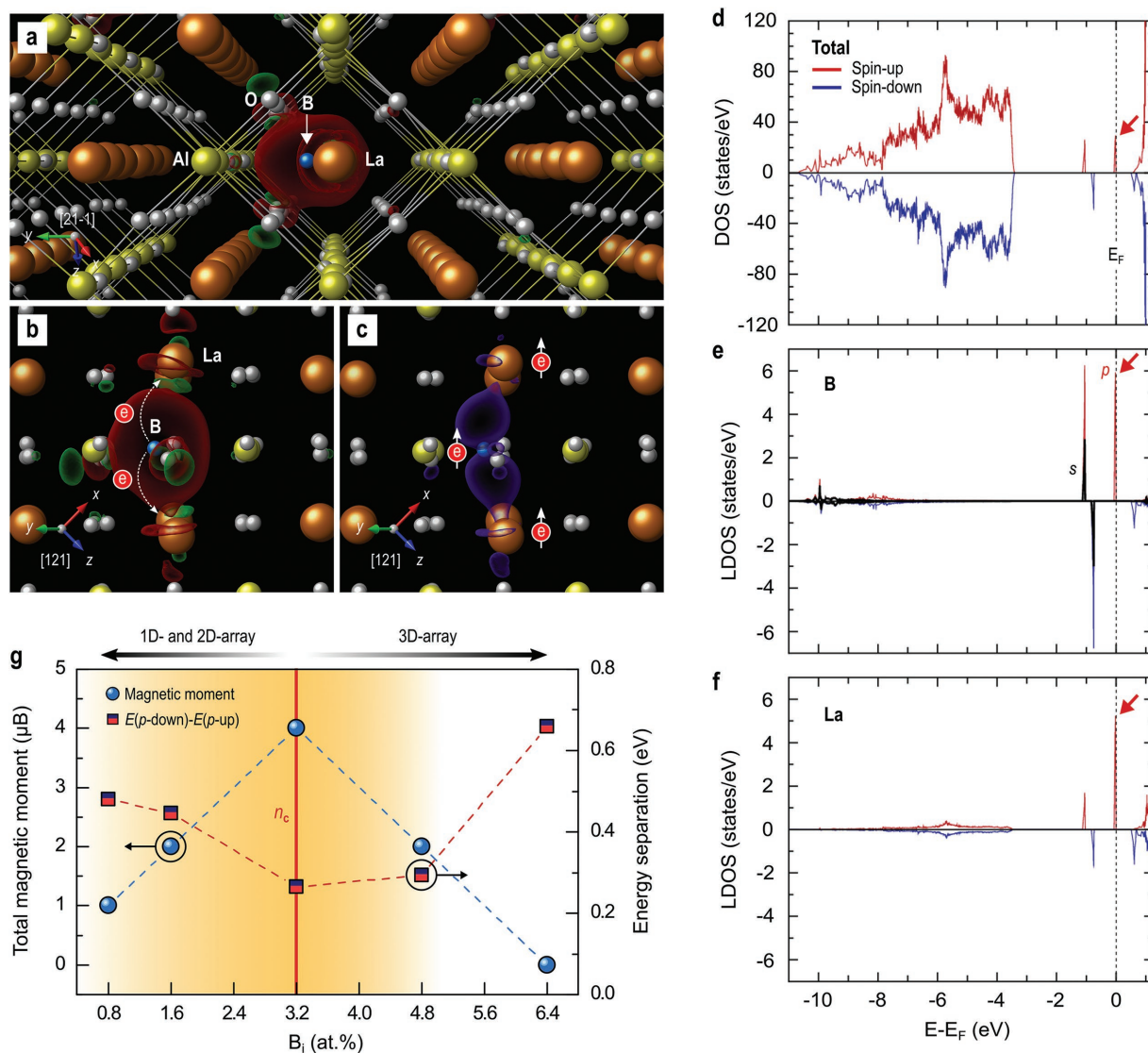


Figure 4. The charge density difference of a relaxed AIRSS-derived LAO supercell (SC) with a B_i (≈ 0.8 at%), projected along the a) $\langle 21\bar{1} \rangle_R$ and b) $\langle 121 \rangle_R$ zone axes. The isosurface value is taken as $8 \times 10^{-3} \text{ eV } \text{\AA}^{-3}$. c) The spin charge imbalance from the spin polarization states of the B_i :LAO SC projected along the $\langle 121 \rangle_R$ zone axis. d) The total and spin-polarized DOS of the B_i :LAO SC. The s- and p-projected spin-resolved local density of states of e) B_i and f) La. g) Variations in the total magnetic moments and energy separation of B_i p states—energy difference, $\Delta E = E$ (unoccupied p-states of B_i above the E_F) $- E$ (B_i occupied p-states of B_i near the E_F), as a function of the number of B_i , aligned periodically within the x - y - z coordination of the SCs. In the LAO SCs, the B interstitials were calculated to be aligned, separating B_i individuals into each LAO UC along the uni- and planar directions until the B_i atomic concentration, $n_C = 3.2$ at%. 3D alignment of B_i in the LAO SCs was made above n_C .

alignment of the spin-polarized electrons between the B_i and La cations through the hybridization of the p - d band as shown in Figure 4c.

Our calculations further show no change in the electronic and magnetic properties of the B_i :LAO system by the presence of oxygen vacancy nearby the B_i , and no magnetization of the system caused by a B-pair (a B dimer) within the LAO SC as shown in Figures S10b and S11 (Supporting Information). These results suggest that clustering of B_i atoms needs to be minimized to secure the Stoner-type exchange interaction between the itinerant electrons (impurity band spin-split), and subsequent spin polarization with the nearest neighbors. Hence, a unidirectional/planar array of isolated

B individuals along rhombohedral LAO lattices is the key feature for tailoring both the magnetization and conductivity of the LABO composites until a percolation threshold concentration of B_i , $n_C = 3.2$ at% as illustrated in Figure 4g and Figure S12 (Supporting Information). In conjunction, depreciated magnetic and electrical responses were measured in the composite samples, with a largely disordered host system, and thus the effective interstitial doping level needs to be driven over a limited range below the percolation threshold concentration. This is also reflected in the measurements, as the EF-LABO($x = 8\%$) exhibits comparatively lower saturation magnetization, when compared to the EF-LABO($x = 3\%$) composite (Figure 3d).

The striking phenomenon observed in this study is that trivalent B_i effectively contributes excessive spin-polarized electrons primarily to the neighboring same charge-valent La cations in the LAO lattices. The delicate positioning of B_i in between two La ions could be perceived to be driven by the electronegativity difference between the two cations (B and La), which is around $\Delta\chi_e = 0.86$, against the typical ionic attraction between B and O. Namely, a stronger ionization force between La and O in the host LAO lattices prevents B_i -O bonds, which maintains the position of B interstitials. This eventually results in the La- B_i -La interactions, giving rise to spin-polarized charge transfer. The proposed mechanism was henceforth analyzed using thin films of LBO that were grown on different nonmagnetic oxide crystals, namely pseudocubic $LaAlO_3(001)_{pc}$, $STO(001)$, and $MgO(001)$. As expected, our results clearly show that the nonmagnetic oxides turn over high-temperature ferromagnets due to interdiffused B interstitials (Figure S13, Supporting Information). Consequently, the following conditions, i.e., a large difference in electronegativities, hybridization and ordering of interstitial states, and charge neutrality level in ionic material systems,^[46,11] can firmly assist in functional interstitial light element doping.

In summary, we report an intriguing, yet straightforward approach to engineer functional properties, namely resistive switching and high-temperature ferromagnetic response, by interstitial light element doping in a novel composite oxide system. A large electronegativity difference between the B and La cations in the host LAO lattices preserves effective interstitial B doping, which is critical for the reconstruction of the electronic states and magnetization of the composite system used in this study. The eventual tunability of the induced effects via the rearrangement of B_i by an external stimulus proves the robustness of the mechanism, and its potential utility in a host of other bulk oxide dielectric materials, which is validated by the result of thin film synthesis. The proposed mechanism, therefore, has a universal character and can be explored with different combinations of heavy and light element cations in ionic compound materials systems. The adopted route predominantly takes impact of the interstitial doping, in contrast to the widely employed substitutional doping. Our findings offer a pathway to engineer a new class of bulk oxide materials with light element interstitial dopants for desirable ionic/electronic and magnetic characteristics in oxide-based electronic and energy applications.

Supporting Information

Supporting Information is available from the Wiley Online Library or from the author.

Acknowledgements

The authors acknowledge the financial support from the DFG through Sonderforschungsbereiche 762 (Grant No. A12). This work was partially supported by the Bundesministerium für Bildung und Forschung fund (Grant No. 03Z22HN12). Prof. S. Ebbinghaus in the Institut für Chemie, Martin-Luther-Universität Halle-Wittenberg and Prof. M. Alexe in the department of Physics, University of Warwick are thanked for technical support for this work. A.J.M. acknowledges the support from the Winton Programme for the Physics of Sustainability.

Conflict of Interest

The authors declare no conflict of interest.

Keywords

first-principle calculations, light element interstitial doping, oxide composites, resistive switching, Stoner ferromagnetism

Received: March 29, 2018

Revised: July 5, 2018

Published online: August 21, 2018

- [1] S. Jin, T. H. Tiefel, M. McCormack, R. A. Fastnacht, R. Ramesh, L. H. Chen, *Science* **1994**, 264, 413.
- [2] A. Ohtomo, M. Kawasaki, T. Koida, K. Masubuchi, H. Koinuma, *Appl. Phys. Lett.* **1998**, 72, 2466.
- [3] I. Grinberg, D. Vincent West, M. Torres, G. Gou, D. M. Stein, L. Wu, G. Chen, E. M. Gallo, A. R. Akbashev, P. K. Davies, J. E. Spanier, A. M. Rappe, *Nature* **2013**, 503, 509.
- [4] J. Wang, J. B. Neaton, H. Zheng, V. Nagarajan, S. B. Ogale, B. Liu, D. Viehland, V. Vaithyanathan, D. G. Schlom, U. V. Waghmare, N. A. Spaldin, K. M. Rabe, M. Wuttig, R. Ramesh, *Science* **2003**, 299, 1719.
- [5] J. H. Haeni, P. Irvin, W. Chang, R. Uecker, P. Reiche, Y. L. Li, S. Choudhury, W. Tian, M. E. Hawley, B. Craigo, A. K. Tagantsev, X. Q. Pan, S. K. Streiffer, L. Q. Chen, S. W. Kirchoefer, J. Levy, D. G. Schlom, *Nature* **2004**, 430, 758.
- [6] R. Waser, M. Aono, *Nat. Mater.* **2007**, 6, 833.
- [7] B. W. Veal, S. K. Kim, P. Zapol, H. Iddir, P. M. Baldo, J. A. Eastman, *Nat. Commun.* **2016**, 7, 11892.
- [8] D. Kan, T. Terashima, R. Kanda, A. Masuno, K. Tanaka, S. Chu, H. Kan, A. Ishizumi, Y. Kanemitsu, Y. Shimakawa, M. Takano, *Nat. Mater.* **2005**, 4, 816.
- [9] H. Kaftelen, K. Ocakoglu, R. Thomann, S. Tu, S. Weber, E. Erdem, *Phys. Rev. B* **2012**, 86, 014113.
- [10] H. N. Lee, H. M. Christen, M. F. Chisholm, C. M. Rouleau, D. H. Lowndes, *Nature* **2005**, 433, 395.
- [11] J. L. MacManus-Driscoll, P. Zerrer, H. Wang, H. Yang, J. Yoon, A. Fouchet, R. Yu, M. G. Blamire, Q. Jia, *Nat. Mater.* **2008**, 7, 314.
- [12] A. Ohtomo, H. Y. Hwang, *Nature* **2004**, 427, 423.
- [13] D. A. Dikin, M. Mehta, C. W. Bark, C. M. Folkman, C. B. Eom, V. Chandrasekhar, *Phys. Rev. Lett.* **2011**, 107, 056802.
- [14] C. Chappert, A. Fert, F. N. Van Dau, *Nat. Mater.* **2007**, 6, 813.
- [15] A.-M. Haghiri-Gosnet, J.-P. Renard, *J. Phys. D: Appl. Phys.* **2003**, 36, R127.
- [16] K.-I. Kobayashi, T. Kimura, H. Sawada, K. Terakura, Y. Tokura, *Nature* **1998**, 395, 677.
- [17] M. Gibert, P. Zubko, R. Scherwitzl, J. Iiguez, J.-M. Triscone, *Nat. Mater.* **2012**, 11, 195.
- [18] X. R. Wang, C. J. Li, W. M. Lü, T. R. Paudel, D. P. Leusink, M. Hoek, N. Poccia, A. Vailionis, T. Venkatesan, J. M. D. Coey, E. Y. Tsymlal, Ariando, H. Hilgenkamp, *Science* **2015**, 349, 716.
- [19] P. Moetakef, J. R. Williams, D. G. Ouellette, A. P. Kajdos, D. Goldhaber-Gordon, S. J. Allen, S. Stemmer, *Phys. Rev. X* **2012**, 2, 021014.
- [20] W. S. Choi, J.-H. Kwon, H. Jeon, J. E. Hamann-Borrero, A. Radi, S. Macke, R. Sutarto, F. He, G. A. Sawatzky, V. Hinkov, M. Kim, H. N. Lee, *Nano Lett.* **2012**, 12, 4966.
- [21] A. Asamitsu, Y. Tomioka, H. Kuwahara, Y. Tokura, *Nature* **1997**, 388, 50.
- [22] L. Yao, S. Inkinen, S. van Dijken, *Nat. Commun.* **2017**, 8, 14544.

- [23] P. Perna, D. Maccariello, F. Ajejas, R. Guerrero, L. Méchin, S. Flament, J. Santamaria, R. Miranda, J. Camarero, *Adv. Funct. Mater.* **2017**, 27, 1700664.
- [24] E. Erdem, R. Böttcher, H.-J. Gläsel, E. Hartmann, *Magn. Reson. Chem.* **2005**, 43, S174.
- [25] W. J. Kim, J. H. Leem, M. S. Han, I.-W. Park, Y. R. Ryu, T. S. Lee, *J. Appl. Phys.* **2006**, 99, 096104.
- [26] D.-S. Park, H. Wang, S. K. V. Farahani, M. Walker, A. Bhatnagar, D. Seghier, C.-J. Choi, J.-H. Kang, C. F. McConville, *Sci. Rep.* **2016**, 6, 18449.
- [27] I. J. Beyerlein, M. J. Demkowicz, A. Misra, B. P. Uberuaga, *Prog. Mater. Sci.* **2015**, 74, 125.
- [28] L. Zhong, X. H. Liu, G. F. Wang, S. X. Mao, J. Y. Huang, *Phys. Rev. Lett.* **2011**, 106, 48302.
- [29] D. P. Young, D. Hall, M. E. Torelli, Z. Fisk, J. L. Sarrao, J. D. Thompson, H.-R. Ott, S. B. Oseroff, R. G. Goodrich, R. Zysler, *Nature* **1999**, 397, 412.
- [30] R. Hhne, P. Esquinazi, *Adv. Mater.* **2002**, 14, 753.
- [31] D. M. Edwards, M. I. Katsnelson, *J. Phys.: Condens. Matter* **2006**, 18, 7209.
- [32] J. M. D. Coey, P. Stamenov, R. D. Gunning, M. Venkatesan, K. Paul, *New J. Phys.* **2010**, 12, 053025.
- [33] J. H. Lee, I. Fina, X. Marti, Y. H. Kim, D. Hesse, M. Alexe, *Adv. Mater.* **2014**, 26, 7078.
- [34] A. Herklotz, A. T. Wong, T. Meyer, M. D. Biegalski, H. N. Lee, T. Z. Ward, *Sci. Rep.* **2016**, 6, 26491.
- [35] S.-G. Lim, S. Kriventsov, T. N. Jackson, *J. Appl. Phys.* **2002**, 91, 4500.
- [36] J. Ma, Q. Wu, Y. Ding, *J. Am. Ceram. Soc.* **2007**, 90, 3890.
- [37] J. J. van der Klink, H. B. Brom, *Prog. Nucl. Magn. Reson. Spectrosc.* **2000**, 6, 89.
- [38] A. Chroneos, R. V. Vovk, I. L. Goulatis, L. I. Goulatis, *J. Alloys Compd.* **2010**, 494, 190.
- [39] K. M. Kim, D. S. Jeong, C. S. Hwang, *Nanotechnology* **2011**, 22, 254002.
- [40] E. Linn, R. Rosezin, C. Kögeler, R. Waser, *Nat. Mater.* **2010**, 9, 403.
- [41] M. Sepioni, R. R. Nair, S. Rablen, J. Narayanan, F. Tuna, R. Winpenny, A. K. Geim, I. V. Grigorieva, *Phys. Rev. Lett.* **2010**, 105, 207205.
- [42] J. M. D. Coey, M. Venkatesan, P. Stamenov, *J. Phys.: Condens. Matter* **2016**, 28, 485001.
- [43] E. F. Kneller, F. E. Luborsky, *J. Appl. Phys.* **1963**, 34, 656.
- [44] B. Arun, M. V. Suneesh, M. Vasundhara, *J. Magn. Magn. Mater.* **2016**, 418, 265.
- [45] C. J. Pickard, R. J. Needs, *J. Phys.: Condens. Matter* **2011**, 23, 053201.
- [46] P. D. C. King, T. D. Veal, D. J. Payne, A. Bourlange, R. G. Egdell, C. F. McConville, *Phys. Rev. Lett.* **2008**, 101, 116808.